Earthquake Engineering & Structural Dynamics
The Journal of the International Association for Earthquake Engineering

EARTHQUAKE ENGINEERING & STRUCTURAL DYNAMICS
Earthquake Engng Struct. Dyn. 2017; **46**:117–137
Published online 7 July 2016 in Wiley Online Library (wileyonlinelibrary.com). DOI: 10.1002/eqe.2777

Shake table test and numerical study of self-centering steel frame with SMA braces

Canxing Qiu[1,2] and Songye Zhu[2,*,†]

[1]*School of Civil Engineering, Shandong University, Jinan 250061, Shandong, China*
[2]*Department of Civil and Environmental Engineering and Research Institute for Sustainable Urban Development, The Hong Kong Polytechnic University, Hung Hom, Kowloon, Hong Kong*

SUMMARY

Given their excellent self-centering and energy-dissipating capabilities, superelastic shape memory alloys (SMAs) become an emerging structural material in the field of earthquake engineering. This paper presents experimental and numerical studies on a scaled self-centering steel frame with novel SMA braces (SMAB), which utilize superelastic Ni–Ti wires. The braces were fabricated and cyclically characterized before their installation in a two-story one-bay steel frame. The equivalent viscous damping ratio and 'post-yield' stiffness ratio of the tested braces are around 5% and 0.15, respectively. In particular, the frame was seismically designed with nearly all pin connections, including the pinned column bases. To assess the seismic performance of the SMA braced frame (SMABF), a series of shake table tests were conducted, in which the SMABF was subjected to ground motions with incremental seismic intensity levels. No repair or replacement of structural members was performed during the entire series of tests. Experimental results showed that the SMAB could withstand several strong earthquakes with very limited capacity degradation. Thanks to the self-centering capacity and pin-connection design, the steel frame was subjected to limited damage and zero residual deformation even if the peak interstory drift ratio exceeded 2%. Good agreement was found between the experimental results and numerical simulations. The current study validates the prospect of using SMAB as a standalone seismic-resisting component in critical building structures when high seismic performance or earthquake resilience is desirable under moderate and strong earthquakes.

Received 12 August 2015; Revised 23 May 2016; Accepted 30 May 2016

KEY WORDS: shake table test; numerical simulation; shape memory alloys; self-centering; steel braced frame; shape memory alloy brace; earthquake resilience

HIGHLIGHTS

- Conducted shake table tests of self-centering steel frame with novel shape memory alloy braces (SMAB);
- Systematically investigated seismic performance of SMAB frame (SMABF) at different seismic intensity levels through incremental dynamic tests and analyses;
- Experimentally validated the salient features of SMABF, including large recoverable interstory drift ratio, reusability of SMAB for numerous earthquakes, and a nearly damage-free state of the frame under strong earthquakes. Such experimental validation has not been reported in the literature.

*Correspondence to: Songye Zhu, Department of Civil and Environmental Engineering, The Hong Kong Polytechnic University, Hung Hom, Kowloon, Hong Kong
†E-mail: ceszhu@polyu.edu.hk

1. INTRODUCTION

Steel braced frames are common seismic-resisting structural systems. The seismic capacity of steel braced frames can be improved by enhancing structural resisting strength, structural deformation capacity, and energy dissipation capacity. Typical braced frame systems include special concentrically braced frames, eccentrically braced frames, and buckling-restrained braced frames. Moreover, supplemental energy dissipation devices, such as metallic dampers, friction dampers, and viscous dampers, may be implemented to improve the seismic capacity of structures and protect both structural and nonstructural members. Although conventional design strategies can guarantee structural safety by controlling structural damage and preventing structural collapse, noticeable permanent deformation is frequently observed in conventional seismic-resisting structures according to post-earthquake field reconnaissance. A recent investigation suggested that a residual interstory drift ratio beyond 0.5% makes rebuilding a new structure more favorable than retrofitting or repairing a damaged structure [1]. Although not yet prudently stipulated in current seismic provision [2], the significance of post-earthquake residual deformation has been gradually recognized in the past decades with the increasing emphasis on earthquake resilience that requires fast recovery to minimize social and economic impact of earthquakes. Such recognition in turn inspired the development of high-performance seismic-resisting self-centering structures [3–7] to meet the stringent requirement on the residual interstory drift ratio. Among the various types of self-centering structures, shape memory alloy (SMA)-based self-centering structures that take advantage of the appealing superelasticity of SMAs have recently become the subject of increasing interest and research effort.

SMAs refer to a special kind of metallic alloy that can recover from deformation upon heating (shape memory effect) or unloading (superelastic effect) [8, 9]. The most widely used SMA is Ni–Ti. After a proper training process (i.e., cyclic pre-loading), superelastic SMAs possess stable self-centering and energy-dissipating capabilities without leaving residual deformation. The superelastic strain is typically dependent on the types of SMAs and is up to 8% for Ni–Ti wires. The superelastic behavior of SMAs, signified by a flag-shaped hysteresis, is quite different from common material behavior and is therefore of particular interest from the perspective of earthquake engineering. Moreover, SMAs have excellent corrosion resistance and good low-cycle fatigue life [8, 9]. A variety of seismic-resisting self-centering devices or structural members have been developed based on these favorable features of superelastic SMAs [10–26], including SMA base isolators for elevated highway bridges and frames [11, 21], SMA dampers [12], SMA restrainers for bridge retrofitting [14], SMA bars in precast segmental bridge piers [23], etc.

In particular, growing attention has been given to self-centering steel braced frames by utilizing SMA-based devices. For example, Zhang and Zhu [15] proposed installing SMA dampers in a frame through a braced configuration. Li et al. [19] experimentally studied two SMA dampers installed in the first story of a 1/4-scale five-story two-bay frame and observed effective response reduction performance of the SMA dampers. More research works have been dedicated to the direct use of superelastic SMA in bracing elements so that SMA braces (SMABs) can replace conventional braces or buckling-restrained braces (BRB) in a chevron or diagonal brace configuration. Dolce et al. [27] were the first to investigate SMABs in a shake table test of a 1/3.3-scale three-story two-bay reinforced concrete frame, and found that SMABs can effectively reduce interstory drift ratios and protect the frame from damages. Their promising results inspired further research on the seismic performance of steel braced frames with SMABs [28–33]. A series of numerical studies have demonstrated the superior seismic performance of SMA braced frames (SMABFs). For example, Zhu and Zhang [28] developed an SMAB configuration with adjustable hysteretic behavior and demonstrated through numerical analysis that, compared with buckling-restrained braced frames (BRBF), properly designed SMABFs can achieve comparable performance in terms of peak response control, but significantly reduced residual deformation after earthquakes. Similarly, McCormick et al. [29] numerically illustrated the effectiveness of SMAB in limiting peak and residual interstory drift ratios in concentrically braced steel frames. Motahari et al. [30] examined the effectiveness of SMA braces in a steel braced frame in terms of the prevention of structural and non-structural damage. Yang et al. [31] proposed a SMA-based hybrid brace that processes excellent

DOI: 10.1002/eqe

recentering capability and comparable damping performance to BRB. Moradi et al. [32] evaluated the seismic performance of SMABFs through incremental dynamic analysis (IDA). SMAB not only reduces seismic demand but also generates a uniform response along the building height. Qiu and Zhu [33] found that increasing the post-yield stiffness of SMAB benefits seismic response control performance by limiting the high-mode effect. Compared with the numerical simulations, the relevant experimental studies, particularly the experimental tests of frames, remain relatively limited. Speicher et al. [34] developed a novel SMA brace using helical springs or Belleville washers. The braces produced good self-centering and damping capability in the cyclic tests. Miller et al. [35] combined SMA rods with BRB to form a self-centering BRB, which demonstrated appreciable energy dissipation and self-centering ability in the tests. Boroschek et al. [36] indicated that the peak displacement can be noticeably reduced by installing SMA wires into a rigid steel frame. Ozbulut et al. [37] optimized SMA bracing elements using genetic algorithm and verified its effectiveness by conducting shake table tests. Relevant research remains active in this field. Song et al. [38] and Ozbulut et al. [39] offered comprehensive reviews of the versatile applications of SMAs in civil engineering.

The superior seismic performance of SMABF includes the following: (i) The good superelasticity of SMA enables the frames to be deformed to a larger interstory drift ratio without significant damage than conventional braced frames. (ii) The self-centering characteristics of SMAB minimize the residual deformation of the frames even if the frames experience large peak deformation under severe earthquakes. (iii) The repeatable superelastic behavior makes SMAB reusable after severe earthquakes without the need for replacement. Consequently, the frame can sustain a series of mainshock and aftershocks without significant performance deterioration. (iv) A properly designed SMABF can remain nearly damage-free under small and moderate earthquakes and sustain very limited damage under severe earthquakes. Although these advantages have been illustrated through past numerical simulations to a certain degree of success, supportive experimental studies for such high performance can be rarely found. To address this knowledge gap, the current study presents the shake table tests of a 1/4-scaled two-story one-bay steel frame with diagonal SMABs, of which the kernel component is superelastic Ni–Ti wires. The design and fabrication of the tested SMABF are introduced. The seismic performance of the SMABF is assessed through two series of incremental dynamic tests, in which the frame is subjected to ground motions with incremental intensity levels, including typical near-fault ground motion records. The seismic demand and damage of the frame are experimentally evaluated with respect to various response indices and are further compared with numerical simulation results. In particular, no repair or replacement is conducted during the intervals between the tests to examine the ability of SMABF to resist several strong earthquakes. The presented experimental and numerical study not only validates the aforementioned advantages of SMABF, but also provides a more in-depth understanding of the seismic performance of SMABF under multiple seismic hazard levels.

2. DESIGN OF THE TESTED FRAME

2.1. Prototype frame

As an emerging type of seismic-resisting structure, SMABF is yet to be given a well-developed design methodology. A prototype SMABF is designed in this study by following the traditional design method for BRBF [2]. Figure 1 shows the perspective and plan views of the prototype frame, which is a two-story steel frame with five bays in each direction. The story height and bay width are 4.0 and 6.0 m, respectively. In each direction, there are a total of six braced bays to resist seismic lateral force, whereas the other bays undertake vertical gravity load only. The seismic mass is taken as 91 kg/m^2, which is selected in consideration of the testing capacity of the shake table. Consequently, the floor mass of the frame is 82 tons, and the tributary floor mass for a one-bay braced frame is equal to 13.6 tons. The frame is assumed to be located on a Class D site as defined in [2].

A force-based design method specified in the American Society of Civil Engineers (ASCE) 7-10 [2] is adopted for the prototype SMABF. Table I summarizes the main design parameters used. The fundamental period of the two-story SMABF is estimated to be 0.35 s. The design base shear and

DOI: 10.1002/eqe

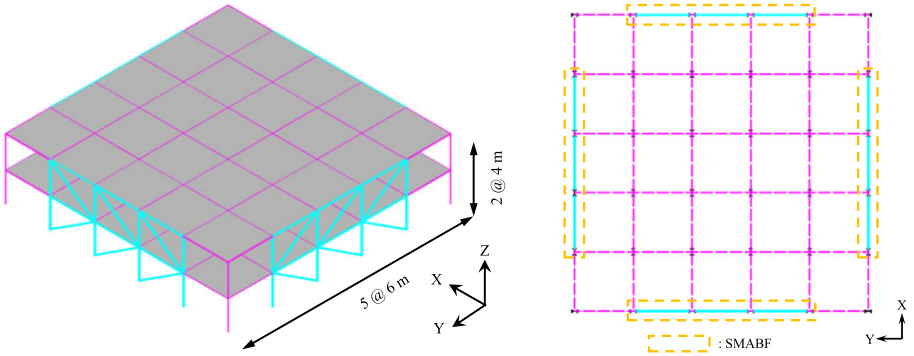

Figure 1. Perspective and plan views of the prototype frame.

Table I. Seismic design parameters of SMABF prototype.

Design parameters	Value
Seismic design category	D
Redundancy factor, ρ	1.3
Occupancy category	II (Office)
Importance factor	
Damping ratio	5%
Mapped spectral acceleration at short-periods, S_S	2.0 g
Mapped spectral acceleration at 1-sec period, S_1	0.707 g
Damping coefficients	$B_S = 1.0$, $B_1 = 1.0$
Site coefficients	$F_a = 1.0$, $F_v = 1.5$
Response modification coefficient, R	7
Overstrength factor, Ω_o	2
Deflection amplification factor, C_d	5½

equivalent lateral force are determined according to the provisions in [2]. The yield strength of the designed braces is equal to 160.3 and 106.9 kN in the first and second floors, respectively. Notably, the strength reduction factor that accounts for strength variability is not applied in the brace design, because of the following facts: (i) the strength reduction factor should be derived from a large number of material or device tests, but very limited testing results of SMAB are available at present; and (ii) the two braces were cyclically tested on an MTS machine before the installation in the frame. So their actual strength is accurately known and the likely variability in the brace strength could be minimized.

In particular, all the beam-to-column connections and column bases are designed to be non-moment-resisting connections. It is noteworthy that the design of the self-centering structures is not specified in existing seismic provisions; the design parameters for BRBF are approximately taken in this study, such as the period parameters C_t and x, response modification coefficient R, deflection amplification factor C_d, and overstrength factor Ω_0. However, by no means does this imply that the SMABF exhibits seismic behavior similar to BRBF. Apparent differences in hysteresis loops and post-yield stiffness ratios, both of which may affect seismic performance, have been noticed between BRBF and SMABF in past studies (e.g. [16, 32]). Although the development of a design methodology for self-centering structures is beyond of the scope of this experimental study, it should be regarded as an urgent task in future studies.

2.2. *Scaled tested frame*

A 1/4-scale SMABF is designed for the shake table test. The full-scale prototype frame is scaled down according to the similitude law presented in Table II. According to the scaling factors, the story height and bay width of the tested model are equal to 1.0 and 1.5 m, respectively. The floor mass is equal to 850 kg, and the yield strength of SMABs is equal to 10.02 and 6.68 kN for the first and second floors, respectively.

DOI: 10.1002/eqe

Table II. Similitude laws used for the reduced model.

Quantities	Scaling factor, S = model / prototype
Length	$S_L = 1/4$
Modulus of elasticity	$S_E = 1$ (same material)
Acceleration/gravity	$S_a = 1$
Force	$S_F = S_E \times S_L^2 = 1/16$
Inertia mass	$S_M = S_F/S_a = 1/16$
Time	$S_T = \sqrt{S_L/S_a} = 1/2$

3. PREPARATION OF THE TESTED FRAME

3.1. SMA wires

Superelastic Ni–Ti wires were purchased from Xi'an Siwei Metal Materials Development Co. Ltd. in China and were selected as the core component in the SMABs. Ni–Ti alloy contains 55.8% titanium in weight percentage. The austenite finish temperature is approximately 0 °C according to the information provided by the supplier. Thus, the Ni–Ti wires exhibit superelasticity at room temperature. The selected Ni–Ti wires can recover from strain up to 6–8% upon unloading. Ni–Ti alloy is also associated with excellent energy dissipation and fatigue properties. In this study, Ni–Ti wires with a diameter of 1.0 mm instead of Ni–Ti bars were used given the easy machinability of Ni–Ti wires. As suggested by [15], the Ni–Ti wires were preloaded for 20 cycles to stabilize the hysteresis before their formal use in the brace. The slight accumulation of residual deformation and slight variation of hysteretic loops in initial loading cycles, often known as the 'training' effect, can be eliminated by such pre-loading cycles. Figure 2 plots the stress–strain relationship of the 'trained' Ni–Ti wires for ten consecutive cycles at a loading frequency of 2.0 Hz. The corresponding equivalent viscous damping ratio of Ni–Ti wires is 3%. Stable and repeatable hysteretic loops were observed. Some additional tests revealed the cyclic behavior of the Ni–Ti wires is insensitive to loading frequency over the dynamic frequency range of 0.5–4.0 Hz [40].

3.2. SMAB

Two SMABs were fabricated in the laboratory using the aforementioned Ni–Ti wires. Figure 3 shows the kernel part of a brace, which is essentially an SMA damper. The damper consists of two sliding steel blocks, two steel rods, and two groups of Ni–Ti wires. The Ni–Ti wires serve as the kernel of the damper and damping brace. As illustrated in Figure 3(a), two steel rods that run through the slots elongate the Ni–Ti wires and transfer the resisting force between the wires and steel blocks. Figure 3(b) shows the mechanism of the SMA damper. The Ni–Ti wires are always in tension

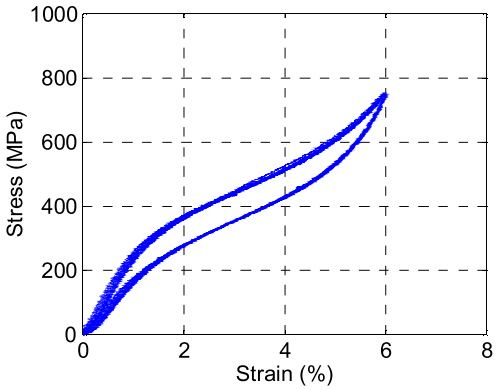

Figure 2. Stress–strain relationship of superelastic Ni–Ti wire (loading frequency of 2.0 Hz, 10 consecutive cycles).

DOI: 10.1002/eqe

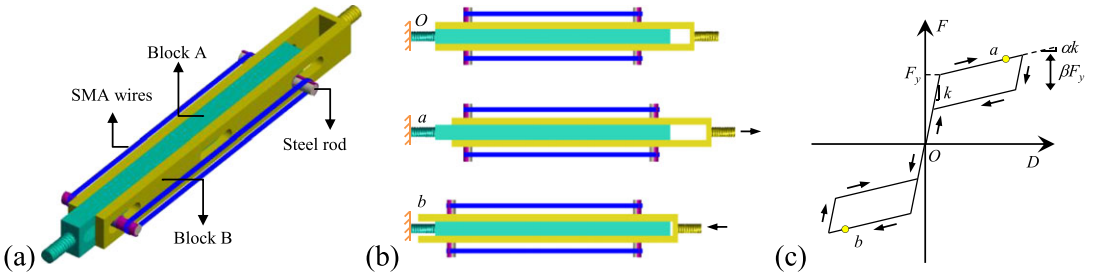

Figure 3. SMA-based damper: (a) configuration of SMA damper, (b) deformation under tension and compression, and (c) idealized flag-shaped hysteresis.

whether or not the damper is subjected to tensile or compressive forces. Such a mechanism enables the efficient use of the Ni–Ti wires. Figure 3(c) plots the idealized flag-shaped hysteretic behavior of the damper, which is similar to other types of self-centering devices. The steel rods are designed to be sufficiently strong to prevent bending deformation. Some cushion material is added on the contact surfaces between the different parts to mitigate the impact that may cause the premature fracture of the Ni–Ti wires.

The wire length is approximately equal to the distance between the two rods, which is prescribed to meet the deformation capacity of SMABs. According to the brace design described in the previous section, the cross section area of the Ni–Ti wires is 33.4 and 22.3 mm^2 for the first- and second-story braces, respectively. The SMABs are designed to remain in elastic range when interstory drift ratios are up to 0.5%. Consequently, the wire length is determined to be 330 mm. Hence the SMABs can recover to nearly zero deformation after unloading from interstory drift ratios of 2.5%. The wire ends are connected using a U-bolt in each loop of the Ni–Ti wires.

Figure 4 shows the configuration and dimensions of the SMAB. The SMAB is composed of the central SMA damper and two extension parts. The middle damper is welded to the two steel square tubes to extend to the desirable length of the brace. The final length of the SMABs is 1360 mm. The braces are connected to the frame using bolts running through the holes on the gusset plates. The

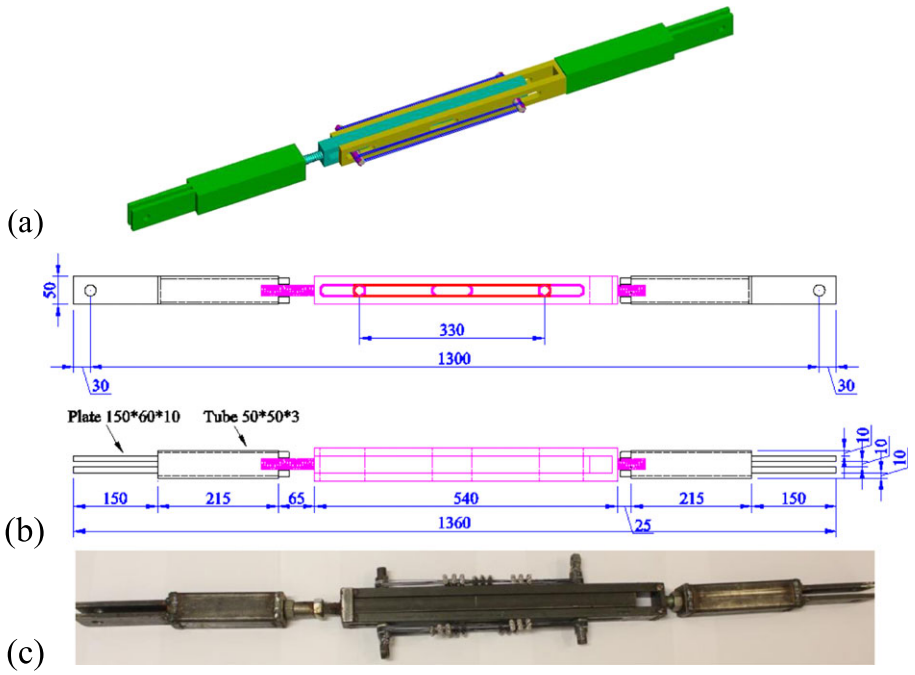

Figure 4. SMA brace (SMAB): (a) schematic view, (b) dimensions (unit: mm), and (c) photo of the tested brace.

DOI: 10.1002/eqe

steel square tubes have a cross section of 50 mm × 50 mm × 3 mm, where 3 mm is the wall thickness. The extension parts are designed to remain elastic so that inelastic deformation is concentrated in the middle segment.

The two SMABs are cyclically tested on an MTS universal testing machine before their installation in the braced frame. Figure 5 shows the cyclic behavior of both the first- and second-story SMABs at a loading frequency of 2.0 Hz. The force–displacement relationships of the tested braces show typical flag-shaped and repeatable hysteresis. However, low initial stiffness is also observed, which is caused by the initial slackness of the wrapped wire loops and the backlash of the fabricated SMABs. The initial slackness is approximately 2 mm, which is less than 1% of the wire length. Such low initial stiffness is certainly undesirable and should be minimized in practice by pre-tensioning the SMA wires and precise machining. Normal elastic stiffness is rapidly gained afterward until the phase transition plateau of the SMA wires. Identified from Figure 5, the equivalent damping ratio and 'post-yield' stiffness of the brace are approximately 5% and 0.15 respectively. The damping ratio of the tested braces (i.e., 5%) is higher than that of SMA wires (i.e., 3%), which is mainly caused by the different strain levels used in the tests shown in Figures 2 and 5. Although the damping capacity is not high, which is common in SMA-based devices, the large 'post-yield' stiffness is very beneficial to limiting seismic response. This is consistent with the prediction in [5]. Table III compares the design target and experimental value of the mechanical properties of the SMABs. The initial stiffness refers to the slope of the elastic loading curve after the slackness. The yield strength is determined from the yield point where the elastic loading slope intersects the post-yield loading slope. The initial stiffness of the tested SMABs agrees with the design targets very well with an error lower than 5%. However, the actual yield strength of SMABs is moderately higher than the design value. The overstrength is mainly because of the non-uniform properties of tensions among different wire loops.

Compared with other types of braces reported in the literature (e.g., BRB in [41] or post-tensioned self-centering energy-dissipative brace in [42]), the SMABs in this study have a relatively smaller strength, mainly because of the limited capacity of the testing facilities in the laboratory. Ni–Ti wires with a diameter of 1 mm are used in the current study. However, the capacity of SMABs in

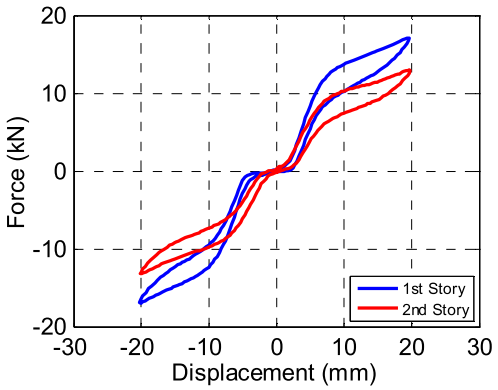

Figure 5. Cyclic behavior of SMAB at a loading frequency of 2.0 Hz.

Table III. Mechanical properties of SMABs.

		SMABs		
		Design	Experimental	Difference
Yield strength (kN)	First story	10.02	11.89	18.6%
	Second story	6.68	8.95	34.0%
Initial stiffness (kN/m)	First story	2410	2530	5.0%
	Second story	1610	1630	1.2%

DOI: 10.1002/eqe

practical applications can be conveniently amplified by using large-diameter SMA wires or bars. Therefore, SMABs are considered scalable and capable of achieving a force level comparable with conventional braces or damping devices.

3.3. *Frame model*

Figure 6(a) shows the elevation view of the scaled structural model tested on the shake table. The structural model consists of two connected parts: a braced frame and a mass simulation frame. The braced frame provides lateral seismic resistance to the entire structural model, and the mass frame simulates the tributary floor mass under earthquakes. The two-story SMABF is mounted on the shake table through pin connections at the column bases, which are different from typically fixed column bases in common braced frames. Figure 6(b) shows a close-up view of the brace-to-frame

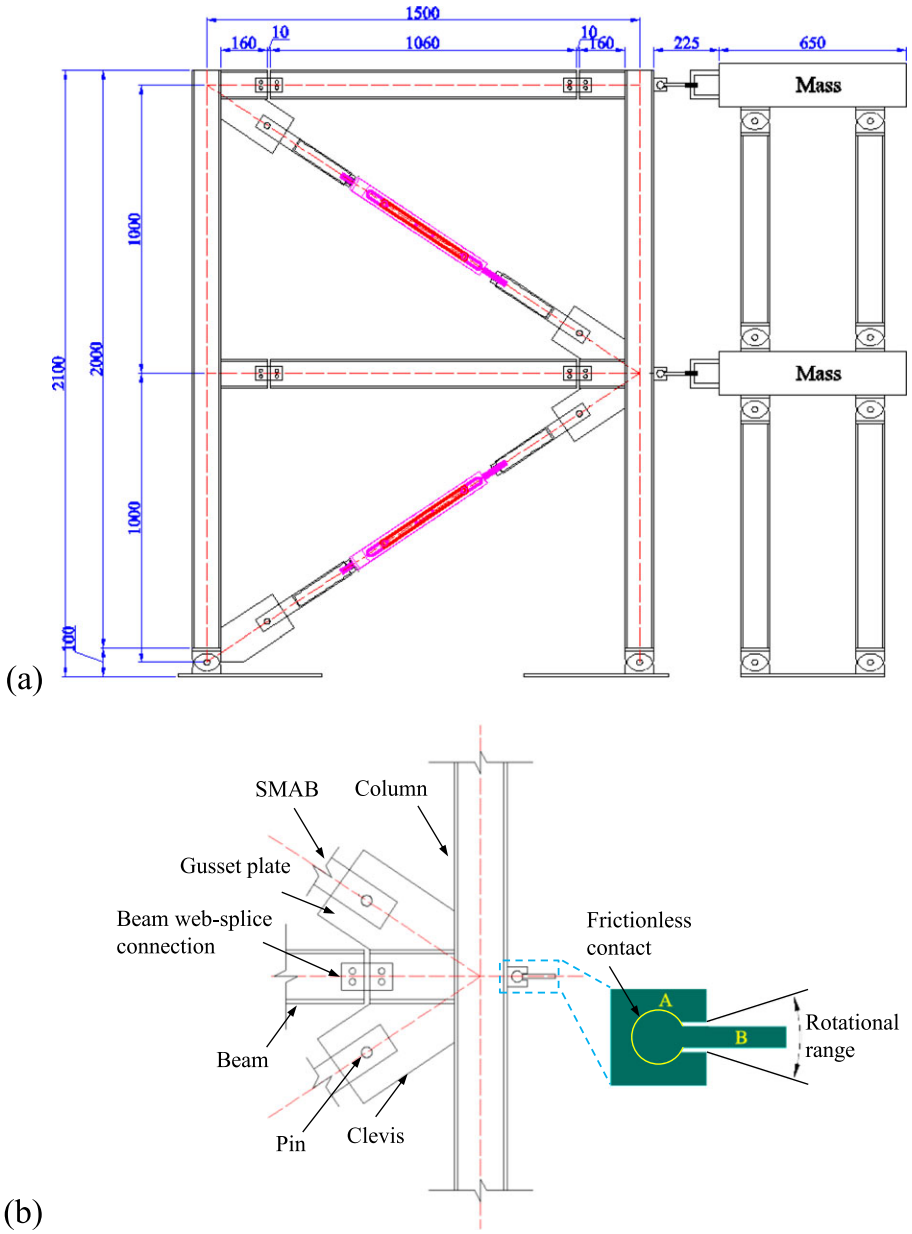

Figure 6. The schematic of the tested SMABF model: (a) elevation view (dimension unit: mm) and (b) close-up view of brace-frame and frame-mass connections.

DOI: 10.1002/eqe

and beam-to-column connections. The brace-to-gusset connection is a true pin connection, which guarantees that the brace undertakes axial force only. A bolted splice plate is utilized to connect beam webs and simulate a beam-to-column connection that mainly transfers axial force with limited flexural constraint. The centerlines of the braces, beams, and columns meet at the same point to eliminate eccentric loads in these members. The pin-connection design in SMABF minimizes the shear force and bending moment in all the frame members and leads to the following characteristics: (i) Axial force becomes the dominant action in the frame members. (ii) Without any moment-resisting frame effect, lateral seismic force is completely resisted by the SMAB elements. (iii) Rotation release allows large lateral deformation of the frame without significant plastic damage.

In the braced bay, the beams and columns have a built-up wide flange section of $H100 \times 50 \times 5 \times 7$ (i.e., depth, width, web thickness, and flange thickness, respectively). Such a section represents nearly the smallest wide flange section commercially available in the local market. The selected section is moderately stronger than that compliant with the similitude law. Because the frame members do not contribute to the lateral force resistance and they remain elastic under the major action of the axial force, the overstrength of the beam and column members imposes very limited influence on the seismic performance of the entire structural system.

In the mass simulation frame, the seismic floor mass (i.e., 850 kg according to the similitude law) is simulated by seven steel plates on each floor level. Figure 7(a) shows a photo of a frame model being tested on the shake table. The floor mass is supported by H-section columns, whose lower and upper ends are both frictionless hinge connections (as shown in Figure 6 (a)). Consequently, the mass simulator is essentially a leaning frame that carries gravity in the vertical direction but does not contribute any lateral resistance in the entire system. The mass simulation frame is connected to the braced frame through a specially designed joint that allows free rotation [Figure 6(b)]. The steel joint consists of Parts A and B, where Part A is welded to the column flange and aligned to the centerline of the beam, and Part B is fabricated by welding a steel cylinder to a steel plate and connected to the mass simulation frame. Such a design allows the relative rotation between two parts with minimal friction. As a result, these connectors constrain the lateral displacements of the two frames at the floor levels and transmit horizontal inertial force to the braced bay without any transmission of vertical load or bending moment. The adoption of the mass simulation frame has the following advantages: (i) It can accommodate a relatively large mass with sufficient space. (ii) It avoids applying unreasonably large axial forces to the columns in the braced bay. (iii) It avoids strengthening the beams in the braced bay by the steel plates. (iv) It offers an appropriate way of simulating the P-Delta effect of seismic inertial forces. Figure 7(b) shows a photo of the connector between the braced frame and mass simulator frame. Figure 7(c) and 7(e) show the connections in the beams and at the column bases.

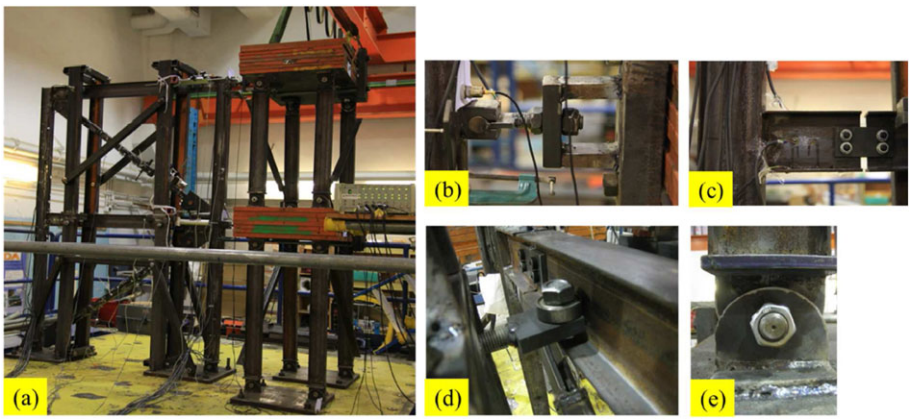

Figure 7. The tested frame on the shake table: (a) global view of the model, (b) pinned connection between the frame and mass system, (c) beam-to-column connection, and (d) ball-bearing of the out-of-plane constraint frame, and (e) pinned joint at the column base.

DOI: 10.1002/eqe

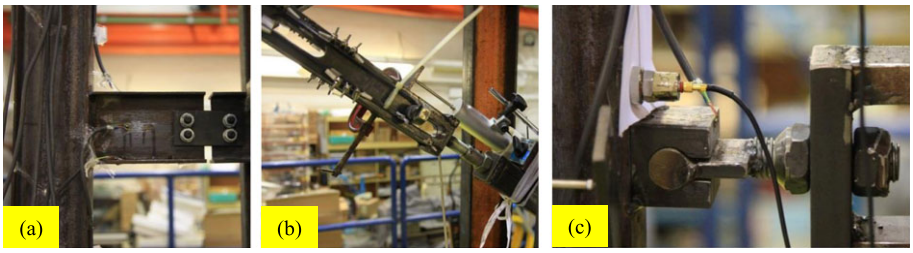

Figure 8. Sensor setup in the shake table test: (a) strain gauge, (b) LVDT, and (c) accelerometer.

In addition to the braced frame and mass simulator frame, another supporting frame is built to prevent the out-of-plane displacement (or even instability) of the braced frame being tested. The ball bearings between the supporting and tested frames provide sufficient out-of-plane constraints but negligible in-plane force to the tested frame. A close-up view of a typical ball bearing is shown in Figure 7(d). As a result, the seismic behavior of the tested SMABF in the ground motion direction can be regarded as unaffected by the supporting frame.

4. EXPERIMENTAL SETUP AND PROGRAM

4.1. Testing apparatus and sensor system

The test was conducted on a 3 m × 3 m unidirectional shake table housed in the Structural Dynamics Laboratory of The Hong Kong Polytechnic University. The maximum ground acceleration of the shake table could reach ±1 g. The MTS feedback control system was calibrated before the formal tests. The calibration could effectively reduce the error of the feedback control system, although discernible errors still existed when input ground motions contained relatively high peak ground acceleration (PGA). Thus, the real ground motions of the shake table were recorded at each test via an accelerometer mounted on the shake table.

A total of 28 strain gauges, 4 linear variable displacement transducers (LVDTs), and 5 accelerometers were used in this experimental study. Figure 8 shows close-up views of some of the installed sensors. The strain gauges were glued on the beams, columns, braces, and force-transmitting connectors to measure their deformation. Two LVDTs were installed between the supporting and tested frames to measure the relative displacement of the tested frame in the direction of ground motion, and the other two were installed on the braces to measure the axial displacement of the braces. The peak and residual deformation and displacement from the strain gauges and LVDTs were closely monitored after running each test, because these indices are related to the structural damage extent. Two accelerometers were installed on each floor level. One was mounted on the right column flange [Figure 8(c)], and the other on the addition mass at the same level. An additional accelerometer was placed on the surface of the shake table to record the actual ground motions to which the tested structural model was subjected. The recorded ground motions were used as the input in the numerical simulations described in the next section. A data acquisition system with a sampling frequency of 2000 Hz was used to record the signals produced by the strain gauges, LVDTs, and accelerometers.

4.2. Ground motions and testing program

Before the formal tests, random and harmonic ground motions of low intensity levels were input to examine the dynamic characteristics (such as the fundamental frequency and damping ratio) of the tested SMABF. Such dynamic characterizations were also performed after the seismic ground motion tests to examine the likely changes of the dynamic characteristics.

In the formal tests, the SMABF was subjected to two series of ground motions. The two ground motions, denoted as LA17 and NF09, were previously developed by Sommerville et al. [43] to represent far- and near-fault ground motions, respectively. The record LA17 corresponds to a design

DOI: 10.1002/eqe

basis earthquake (DBE) in Los Angeles. The information of these two input ground motions is presented Table IV. Figure 9 shows the 5%-damping response spectra of the two ground motions, including the spectral acceleration and displacement demands.

The two ground motions were both scaled to various intensity levels, and the same SMABF was subjected to a series of 'incremental dynamic tests'. Table V presents the series of input ground motions in the real testing order. Such incremental dynamic tests enable the examination of the seismic performance of the SMABF under a wide range of seismic intensities, which cover mild, moderate, and high seismic hazard levels. Among all the tests, Test No. 7 represents the strongest ground motion in which the structural damage under a significant earthquake can be assessed. In the following tests, two scaled-down ground motions were input to examine the seismic performance of the tested frame when subjected to some large aftershock events.

5. NUMERICAL SIMULATION MODEL

Numerical simulations of the tested SMABF were conducted for comparison with the experimental results. The numerical model was built in the computer program OpenSees [44]. Figure 10 shows the modeling details of the tested SMABF. The beams and columns were modeled by force-based

Table IV. Ground motion information.

Record	Name	Station	Year	M	PGA (g)	Distance (km)
LA17	Northridge	Sylmar	1994	6.7	0.57	6.4
NF09	Erzincan	95 Erzincan	1992	6.7	0.43	2.0

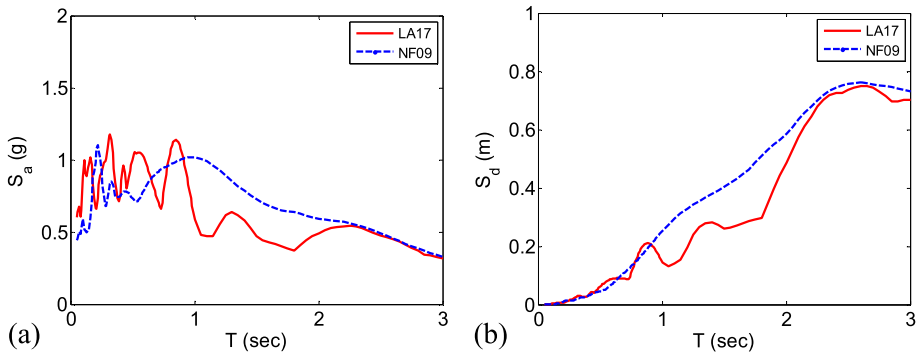

Figure 9. Elastic response spectrum of the selected ground motion records (5% damping ratio): (a) spectral acceleration and (b) spectral displacement.

Table V. Test sequence.

Test no.	Record	Scalar	PGA (g)
1	LA17	0.25	0.14
2	LA17	0.50	0.29
3	NF09	0.25	0.11
4	NF09	0.50	0.22
5	LA17	1.00	0.57
6	NF09	1.00	0.43
7	LA17	1.50	0.89
8	LA17	0.75	0.43
9	NF09	0.75	0.32

DOI: 10.1002/eqe

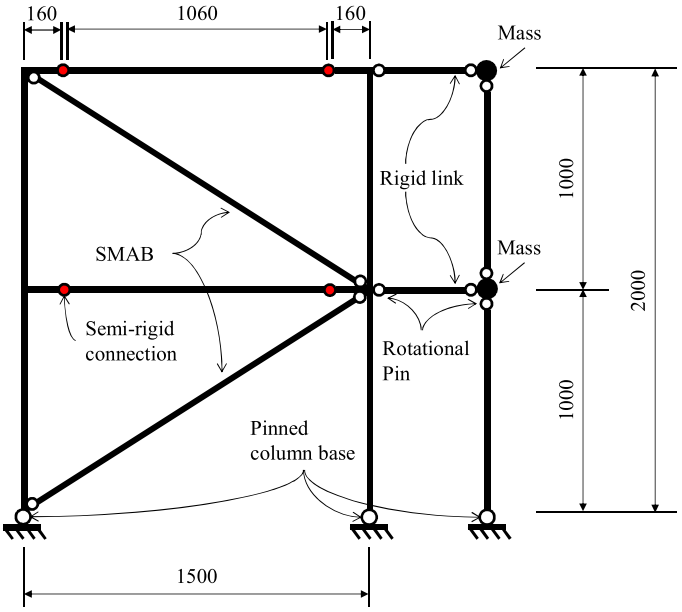

Figure 10. Numerical model of the SMABF in OpenSees (unit: mm).

beam–column elements. The columns were pinned at their bases and continuous at the first floor level. The beam–column connections were shifted away from the column centerlines and were modeled as semi-rigid connections whose rotational stiffness was determined based on the actual testing configuration. Only the in-plane seismic responses of the frame were analyzed. The torsional response of the frame about the vertical axis was not considered, because the supporting frame constrains the out-of-plane displacement during the tests. The mass simulation frame was idealized as a leaning column. The leaning column was constrained to have the same lateral displacement as the braced bay at the two floor levels. The stiffness and strength of the leaning columns were modeled according to the practical constructions. The leaning column was connected to the floor mass through pin connections. As a result, the leaning column did not contribute any lateral resistance to the entire structural system. P-Delta effect was considered in the dynamic simulations.

Considering no damage or buckling was observed in the bracing elements during the tests, the SMABs were modeled as axially loaded members with the actual length. The required material properties were calculated based on the actual stiffness and strength of the tested braces because the brace length differed from the length of the SMA wires. To accurately capture the cyclic behavior of the SMABs shown in Figure 5, including self-centering behavior and initial slackness, a hybrid material model was introduced, as shown in Figure 11. The new model is essentially a combination of two types of material models: (i) *SelfCentering* material, which properly simulates the flag-shaped hysteresis of SMA materials, and (ii) *ElasticMultiLinear* material, which accounts for the initial slackness in the braces. The bilinear force–displacement relationship of the latter material facilitates

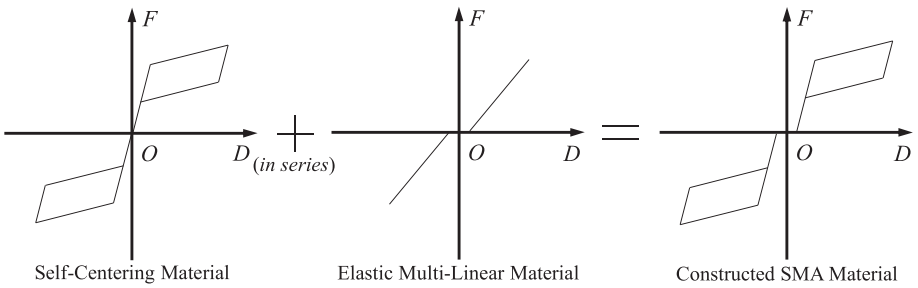

Figure 11. Modeling of the cyclic behavior of SMAB.

DOI: 10.1002/eqe

capturing the initial low stiffness of SMABs shown in Figure 5 and more accurately simulating the seismic behavior of the tested frame model. The initial stiffness and slackness of the bilinear model were calibrated based on the measurement data from the LVDTs in the experiments. These two material models were connected in series to achieve the target cyclic behavior. The *Series* command was used to construct the final constitutive model of the SMABs. A similar treatment was also adopted by Erochko et al. [45] in their modeling of the SCED braces to consider some factors, such as pretension of tendons, slip of friction surface, and contact of end plates.

Rayleigh damping was adopted to account for the inherent damping of the frame structure. The final damping ratio used in the numerical model was given as 4%. Similar to the shake table tests, the IDA of the numerical model was performed under varying seismic intensity levels. The actual ground accelerations recorded in the shake table test were used as the input ground motions.

6. EXPERIMENTAL AND NUMERICAL RESULTS

The results of the shake table tests of SMABF, together with those of the numerical simulations, are presented and discussed in this section. In particular, the seismic performance of SMABF under different seismic intensities is systematically evaluated, which to the best of our knowledge is yet to be reported in the literature. The seismic demands of interest include global responses (such as peak and residual roof displacements, interstory drift, base shear, etc.) and internal loadings of the SMABF model.

6.1. Dynamic characteristics

The dynamic characteristics of the tested SMABF were evaluated when the frame was subjected to random and sine wave excitations. The PGA of the ground motions ranged from 0.01 g to 0.05 g, which induced the elastic behavior of the tested frame. The dynamic characterization indicated that the SMABF model had a fundamental frequency of 2.3 Hz, which was close to the initial estimation in the design stage. The equivalent damping ratio was approximately 4%. A consistent damping ratio was also used in the numerical modeling and simulation.

6.2. Displacement response

Figure 12 shows the time histories of the roof displacement and the corresponding roof drift ratio in all the test cases, where the roof drift ratio refers to the ratio of roof displacement to building height. The figures are presented in the order of ground motion intensities. Satisfactory agreement between the experimental tests and numerical simulations can be observed in Figure 12. Generally, numerical simulations can accurately predict the peak displacement responses in the shake table tests, although noticeable discrepancy is observed in the entire time histories. The vibration duration under seismic record LA17 was typically longer. Thanks to the excellent self-centering capacity provided by the SMABs, the residual displacement was negligible after all the shake table tests, including the cases with highly significant ground motions LA17 × 1.5 and NF09 × 1.0. This result implied that the designed SMABF could withstand a maximum-considered earthquake (MCE) with significantly limited damage and permanent deformation, which could considerably reduce post-earthquake repair cost and downtime.

In real scenarios, a structure may be subjected to a large number of major aftershocks following the mainshock event. For example, 286 major aftershocks (>4.0 Ms) were reported after the Wenchuan Earthquake in China in 2008 [46]. Structural safety under major aftershocks has recently drawn increasing attention from the earthquake engineering community. To investigate this effect, two test cases of LA17 × 0.75 and NF09 × 0.75 were conducted after the test with the most significant ground motion LA17 × 1.5. No repair or modification of the frame was conducted before the two aftershock tests. No residual deformation and performance deterioration were observed in the displacement time histories under LA17 × 0.75 and NF09 × 0.75, demonstrating the potential capability of SMABF to withstand a mainshock and several major aftershocks without the need for major repair.

DOI: 10.1002/eqe

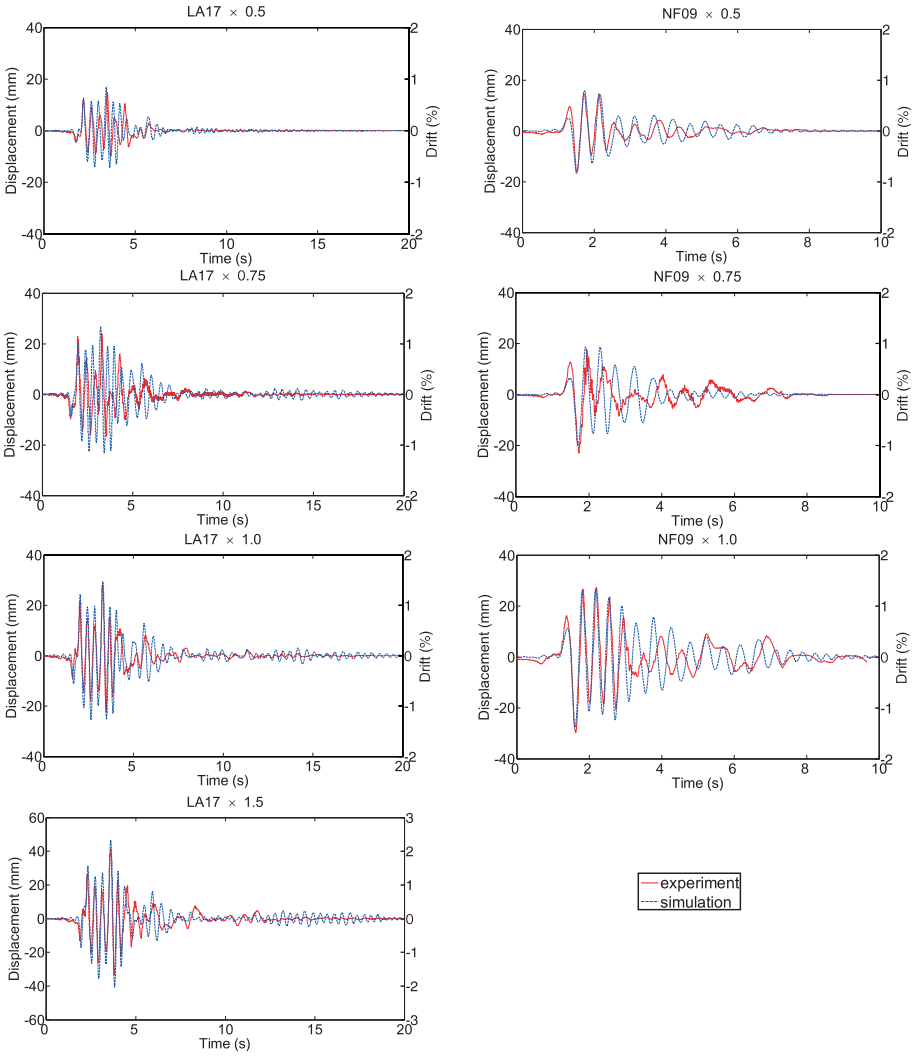

Figure 12. Time histories of the roof displacement, subjected to ground motion records (a) LA17 and (b) NF09 at different seismic intensities.

Figure 13 shows the maximum interstory drift ratios along the frame height for each test case. The relative displacement of the two adjacent floors was calculated from the difference of two LVDT readings installed on the floor levels. In Figure 13(a), the maximum interstory drift ratios are approximately 1.7% and 2.1% at the DBE and MCE seismic hazard levels, respectively. In general, the tested SMABF exhibits a fairly uniform distribution of interstory drift ratios under both ground motions of different intensities. The seismic behavior of the two-story SMABF is dominated by the fundamental vibration mode, and the high-mode effect that may lead to non-uniform interstory drift distribution is not significant in this low-rise building model. The results of the numerical simulations show a satisfactory agreement with the experimental results in both Figures 12 and 13, which justify the efficacy of the numerical model established in the program OpenSees.

6.3. Base shear

Figure 14 shows the time histories of the base shear from the experimental results and numerical simulations for all seismic loading cases. The base shear is calculated as the summation of seismic inertial forces on different floors:

DOI: 10.1002/eqe

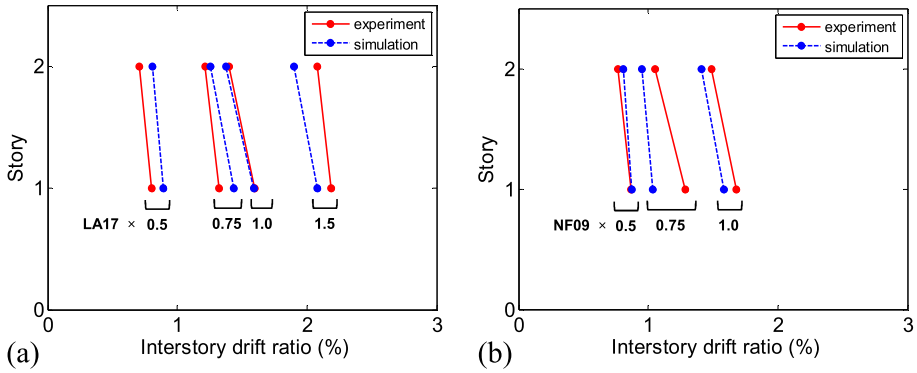

Figure 13. Maximum interstory drift ratio along the building height at different ground motion intensities: (a) LA17 and (b) NF09.

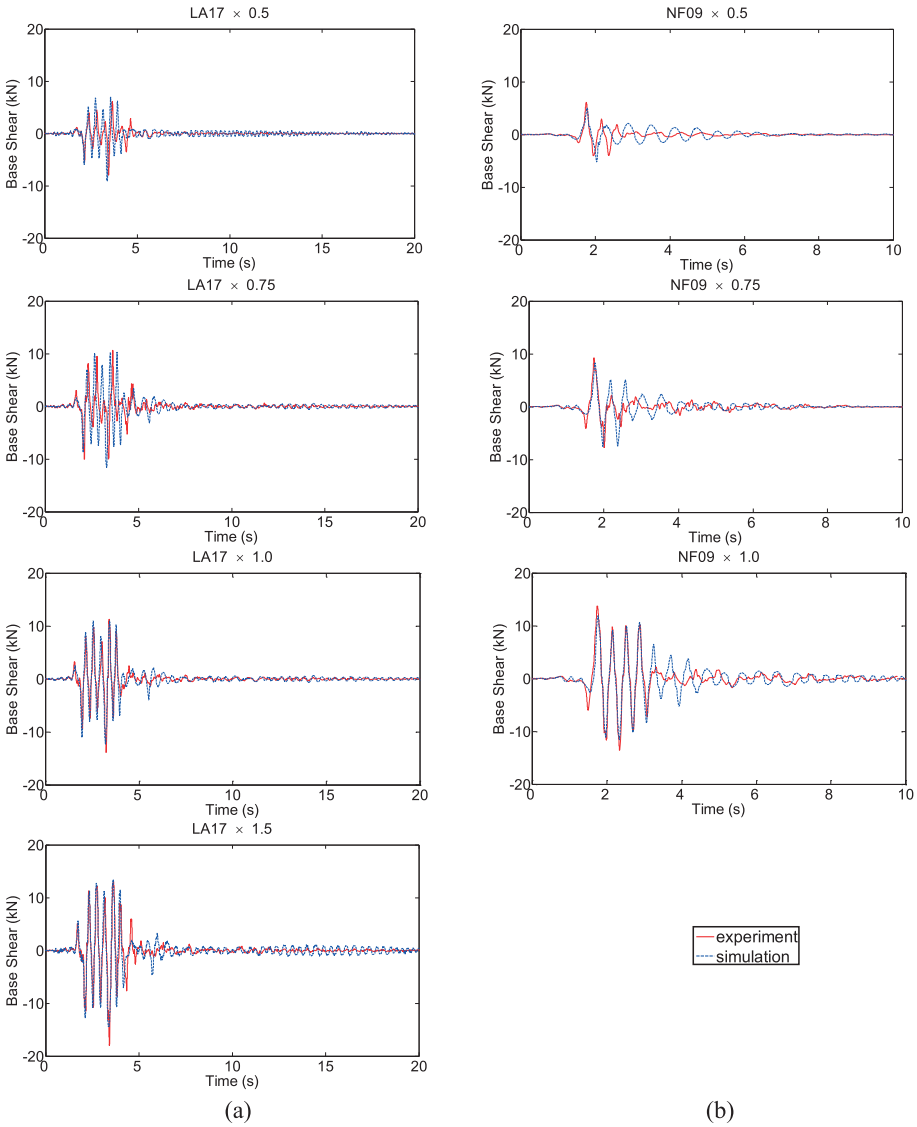

Figure 14. Time histories of the base shear, subjected to ground motion records (a) LA17 and (b) NF09 at different seismic intensities.

DOI: 10.1002/eqe

$$V_{base} = \sum_{i=1}^{2} m_i \cdot a_i \tag{1}$$

where m_i is the floor mass on the ith floor and a_i is the absolute acceleration measured by the accelerometer on the ith floor. Good agreement is again observed between the experimental and numerical results. Generally, the numerical simulations tend to slightly underestimate the base shear in comparison with the shake table test results, which may be attributed to the discrepancy between the experimental hysteresis and numerical constitutive model of SMAB or measurement errors of accelerations. The maximum base shear of 18.0 kN occurs in the strongest loading case of LA17 × 1.5, which is consistent with the cyclic behavior of the SMAB in the first story shown in Figure 5.

6.4. IDA curves

Figure 15 further compares the IDA curves of the peak roof drift ratios, brace displacements, roof accelerations, and base shear from the experimental data and numerical simulations. In the figure, PGA is adopted as the intensity measurement (*IM*) of the scaled ground motions, and the peak roof drift ratios, roof accelerations, and base shear are regarded as a damage measure (*DM*). As shown in Figure 15 (a), the peak roof drift ratio is less than 1.0% under a moderate earthquake (i.e., LA17 × 0.5), and increases to approximately 1.5% and 2.0% in the cases of DBE (i.e., LA17 × 1.0) and MCE (i.e., LA17 × 1.5) earthquakes, respectively. Figure 15 (b) shows the deformation of the first-story brace, which exhibits a similar trend with the roof drift ratio. The second-story brace exhibits a slightly smaller deformation demand than the first-story brace, but the brace deformation between two stories is generally uniform. The peak roof acceleration shown in Figure 15 (c) is approximately 0.5 g under a moderate earthquake and reaches approximately 1.0 and 1.2 g at DBE and MCE levels, respectively. The base shear in Figure 15(d) shows a nearly identical trend with the acceleration, as the base shear can be calculated from the floor accelerations and masses. Furthermore, Figure 15 shows very similar trends under LA17 and NF09. This similarity reveals that the remarkable velocity pulse in the near-fault record NF09 does not exert a negative impact on the studied SMABF in terms of the *DM* shown in Figure 15.

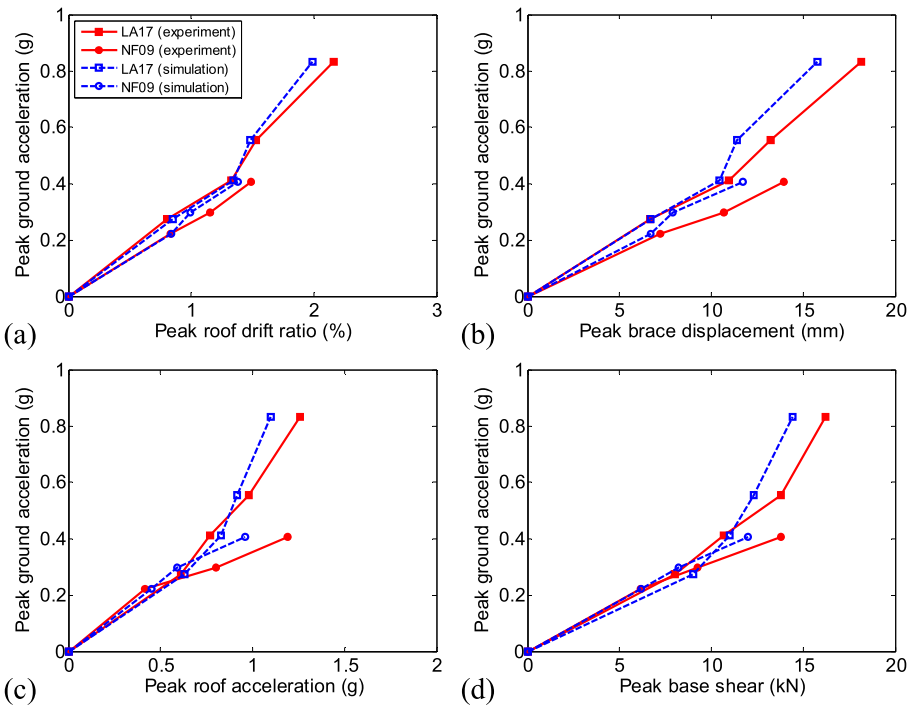

Figure 15. IDA curves: (a) roof drift ratio, (b) first-story brace displacement, (c) roof acceleration, and (d) base shear.

DOI: 10.1002/eqe

6.5. *Truss mechanism*

The internal loadings in the frame members are examined in this section. Figure 16 shows the seismic inertial forces on the frame and the internal loadings at four joints at the instant that the base shear reaches its peak value in the case of LA17 × 1.0. According to Figure 14(a), the peak base shear occurs at $t = 3.3$ s in the experiment and at a slightly different instant in the simulations. To maintain consistency, the internal loadings at $t = 3.3$ s are presented for both the experimental and numerical results in Figure 16. In the numerical simulations, the internal loading of different elements can be directly extracted from the OpenSees model; whereas in the experimental results, the bending moments and axial forces are indirectly calculated from the readings of the strain gauges mounted on two flanges of the H-shaped section. The strain measurement indicates that the deformation is within the elastic range and much lower than the yield stress of steel; thus, Hook's law is applied to calculate the stress from the strain gauge measurement. Subsequently, the normal stress is used to derive the bending moments and axial forces at the measurement locations. Figure 16 presents the internal loadings from both the experimental and numerical results. In the experimental results, shear forces are not available, and axial forces and bending moments are available at the locations with strain gauges. The inertia of the braced frame is omitted in the calculation, given that it is considerably smaller than that produced by the mass simulation frame. Again, satisfactory agreement is found between the experimental data and numerical simulations.

As shown in Figure 16, the braces are subjected only to axial forces. Although shear forces and bending moments are detectable in the steel beam and column members, axial force is still the dominant action. Thus, these structural members are mainly subjected to axial forces, and the entire braced bay behaves in a manner similar to a truss, mainly because of the pin connection design in the tested frame. The truss mechanism is beneficial because it allows large deformation without causing plastic damage in the members. As a result, yielding or local buckling does not occur in the beams and columns even in the most serious cases, such as LA17 × 1.5 and NF09 × 1.0. The inelastic deformation is mainly concentrated in the SMABs and can recover upon unloading because of the superelasticity of the Ni–Ti wires. In the entire test series, no repair of the frame members is conducted, although some sensors are damaged because of inappropriate installation. It clearly demonstrates that a properly designed SMABF can withstand several significant earthquakes and

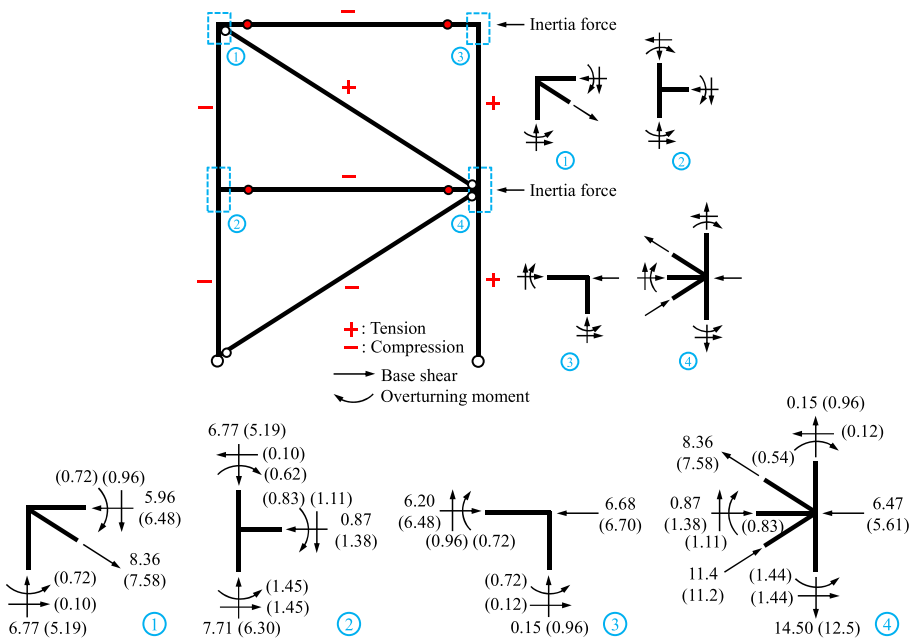

Figure 16. Internal loads of the framing system at the moment when the base shear reaches its maximum, taking the case of LA17 × 1.0 as an example. (Numerical results are enclosed in brackets; unit: kN for force and kN · m for moment).

DOI: 10.1002/eqe

major aftershocks without the need for repair or replacement of any structural members. It is possible to design a self-centering SMABF that is free of structural damage and residual deformation after strong earthquakes.

6.6. *Behavior of SMAB*

Figure 15(b) shows the IDA curves of SMAB displacement. A comparison with Figure 5 reveals the deformation levels of SMAB at different seismic intensity levels. Under a moderate earthquake, the SMAB is in its elastic behavior; as the earthquake intensity increases to DBE and MCE hazard levels, the SMAB undergoes inelastic deformation. Under the most intense earthquake (i.e., LA17 × 1.5), the peak deformation of SMAB is up to 18 mm, which is around 4.2 times the elastic design deformation. The peak brace deformation in the experiment was partially amplified by the initial slackness of SMAB. Based on the peak brace deformation, the peak force of SMAB during the test can be estimated from Figure 5. The peak force of SMAB in the first story is estimated around 15 kN, nearly 1.5 times the design brace force shown in Table III. It is noted that SMABs are subjected to significantly inelastic deformation in this case, but it can still recover from deformation according to Figure 5.

After the completion of all the nine testing cases listed in Table V, the SMABs were removed from the frame and cyclically tested again on the MTS machine. Figure 17 compares the hysteresis behavior of the second-story SMAB before and after the series of shake table tests. The two hysteretic loops are quite consistent with minimal discrepancy in the initial slackness. The stable self-centering cyclic behavior indicates that the SMAB is associated with negligible strength or stiffness degradation after many loading cycles in a series of shake table tests. Thus, well-designed SMABs in a real frame building are reusable without any performance degradation after several earthquakes. This salient feature will make SMABs very appealing in high-risk seismic regions.

7. DISCUSSIONS

Compared with a prior test [27], the current study presents the tests of SMABs in a steel frame and demonstrates that the use of superelastic Ni–Ti alone can achieve satisfactory seismic performance. This experimental study successfully reports some advantages of SMABF that have not been experimentally validated before, In particular, this study examines the seismic performance of SMABF under near-fault ground motions.

The tested SMABs provide a limited damping ratio (5%) and a large ‘post-yield’ stiffness ratio (0.15). The latter is proven effective in limiting seismic responses, as revealed by the shake table tests presented in this study and the previous prediction by others [5]. Notably, semi-rigid or pinned connections are adopted for the beam-to-column connections and column bases in this study. Although different from conventional design in the braced frame, such a pin-connection design is proven a rational design, because it can prevent the occurrence of plastic hinges in the frame that cannot be easily

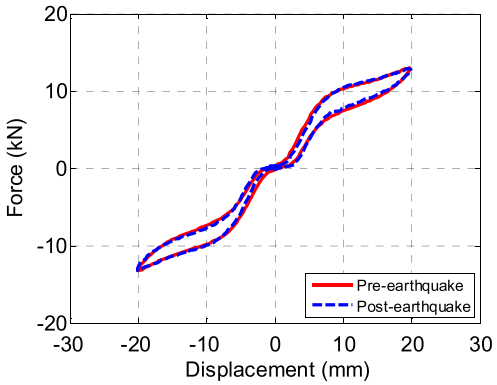

Figure 17. Pre- and post-earthquake performance of the second story SMA-based damper.

DOI: 10.1002/eqe

repaired and allow a large interstory drift ratio. Some similar beam-to-column connections were previously adopted in other types of braced frames as well (e.g. in BRBF [41]).

It is noteworthy that Ni–Ti wires used in the tested SMAB in this study are typically suitable for indoor environments with a relatively stable room temperature. Ni–Ti alloys may not be suitable for outdoor applications because of their sensitivity to temperature [47]. Other types of superelastic SMAs should be considered for outdoor applications, e.g., monocrystalline CuAlBe alloy that has a high superelastic range, large energy dissipation, and excellent low-temperature performance [9].

8. CONCLUSIONS

A seismic-resisting self-centering steel frame with novel SMABs and pin-connection design was investigated experimentally and numerically in this study. In particular, the seismic performance of SMABF was validated through a series of shake table tests on a 1/4-scaled two-story one-bay frame model. Good agreement was observed in the comparisons between the experimental and numerical results. The SMABs enabled the frame to successfully return to the zero position with limited structural damage from a peak interstory drift ratio up to over 2.0%. Such a peak magnitude is considerably larger than those reported in previous experimental studies, and offers important evidence that SMABF, as an emerging type of seismic-resisting structure, can withstand highly intensified seismic hazards.

In the shake table tests, the tested frame model was consecutively subjected to a total of nine ground motion records with incremental intensity levels. The displacement time histories showed that nearly zero residual deformation accumulated after a run of earthquakes. The near-fault earthquakes did not induce an intensified seismic response. The examination of the internal loads in the frame revealed that the axial forces are the dominant actions in the frame and that the existence of SMAB, together with the pin-connection design, forms a desirable truss mechanism that protects the beams and columns against severe damage under severe earthquakes. The numerical simulations showed that the proposed model could properly simulate the cyclic behavior of SMAB and the seismic response of the self-centering braced frame. The time histories of the obtained roof displacement and base shear were compared, and good agreement was achieved between the numerical simulation and experimental data.

The self-centering steel frame with SMABs could sustain several strong earthquakes without severe damage, performance deterioration, or permanent deformation of the frame. The SMABs were also reusable without the need for replacement or repair. These merits of SMABF will considerably reduce the post-earthquake repair cost in comparison with conventional structures. Therefore, the investigated SMABF will be a promising high-performance seismic-resisting structural system when a seismic performance level of immediate occupancy or operation is desired under strong earthquakes.

ACKNOWLEDGEMENTS

The authors are grateful for the financial support of the National Natural Science Foundation of China (Project No. NSFC-51208447) and the Research Institute for Sustainable Urban Development of the Hong Kong Polytechnic University (Project No. 4-ZZCG). The findings and opinions expressed in this paper are solely those of the authors and not necessarily the views of the sponsors.

REFERENCES

1. McCormick J, Aburano H, Ikenaga M, Nakashima M. Permissible residual deformation levels for building structures considering both safety and human elements. Proceedings of the 14th World Conference on Earthquake Engineering, Beijing. China; Paper No. 05-06-0071. 2008.
2. American Society of Civil Engineers (ASCE). *Minimum Design Loads for Buildings and Other Structures, ANSI/SEI7-10*. Reston, Virginia: American Society of Civil Engineers, 2010.
3. Ricles JM, Sause R, Garlock MM, Zhao C. Post-tensioned seismic resistant connections for steel frames. *ASCE Journal of Structural Engineering* 2001; **127**(2):113–121.
4. Christopoulos C, Filiatrault A, Uang CM, Folz B. Post-tensioned energy dissipating connections for moment resisting steel frames. *ASCE Journal of Structural Engineering* 2002; **128**(9):1111–1120.

DOI: 10.1002/eqe

5. Christopoulos C, Filiatrault A, Folz B. Seismic response of self-centering hysteretic SDOF systems. *Earthquake Engineering and Structural Dynamics* 2002; **31**:1131–1150.
6. Erochko J, Christopoulos C, Tremblay R, Kim HJ. Shake table testing and numerical simulation of a self-centering energy dissipative braced frame. *Earthquake Engineering and Structural Dynamics* 2013; **42**(11):1617–1635.
7. Eatherton M, Ma X, Krawinkler H, Deierlein G, Hajjar J. Quasi-static cyclic behavior of controlled rocking steel frames. *ASCE Journal of Structural Engineering* 2014; **140**(11): 04014083. doi. 10.1061/(ASCE)ST.1943-541X.0001005,04014083
8. DesRoches R, McCormick J, Delemont M. Cyclic properties of superelastic shape memory alloy wires and bars. *ASCE Journal of Structural Engineering* 2004; **130**(1):38–46.
9. Qiu C, Zhu S. Characterization of cyclic properties of superelastic monocrystalline Cu–Al–Be SMA wires for seismic applications. *Construction and Building Material* 2014; **72**(15):219–230.
10. Dolce M, Cardone D, Marnetto R. Implementation and testing of passive control devices based on shape memory alloys. *Earthquake Engineering and Structural Dynamics* 2000; **29**:945–968.
11. Wilde K, Gardoni P, Fujino Y. Base isolation system with shape memory alloy device for elevated highway bridges. *Engineering Structures* 2000; **22**(3):222–229.
12. Han YL, Li QS, Li AQ, Leung AYT, Lin PH. Structural vibration control by shape memory alloy damper. *Earthquake Engineering and Structural Dynamics* 2003; **32**:483–494.
13. Andrawes B, DesRoches R. Unseating prevention for multiple frame bridges using superelastic devices. *Smart Materials and Structures* 2005; **14**(3):60–67.
14. Andrawes B, DesRoches R. Effect of ambient temperature on the hinge opening in bridges with shape memory alloy seismic restrainers. *Engineering Structures* 2007; **29**:2294–2301.
15. Zhang Y, Zhu S. A shape memory alloy-based reusable hysteretic damper for seismic hazard mitigation. *Smart Materials and Structures* 2007; **16**(5):1603.
16. Zhu S, Zhang Y. Seismic behavior of self-centering braced frame buildings with reusable hysteretic damping brace. *Earthquake Engineering and Structural Dynamics* 2007; **36**(10):1329–1346.
17. Zhang Y, Zhu S. Seismic response control of building structures with superelastic shape memory alloy wire dampers. *ASCE Journal of Engineering Mechanics* 2008; **134**(3):240–251.
18. Johnson R, Padgett JE, Maragakis ME, et al. Large scale testing of nitinol shape memory alloy devices for retrofitting of bridges. *Smart Materials and Structures* 2008; **17**(3):1–10.
19. Li H, Mao CX, Ou JP. Experimental and theoretical study on two types of shape memory alloy devices. *Earthquake Engineering and Structural Dynamics* 2008; **37**:407–426.
20. Alam MS, Youssef MA, Nehdi M. Analytical prediction of the seismic behavior of superelastic shape memory alloy reinforced concrete elements. *Engineering Structures* 2008; **30**:3399–3411.
21. Casciati F, Faravelli L. A passive control device with SMA components: from the prototype to the model. *Structural Control and Health Monitoring* 2009; **16**(7–8):751–765.
22. Padgett JE, DesRoches R, Ehlinger R. Experimental response modification of a four-span bridge retrofit with shape memory alloys. *Structural Control and Health Monitoring* 2010; **32**(3):165–173.
23. Roh H, Reinhorn AM. Hysteretic behavior of precast segmental bridge piers with superelastic shape memory alloy bars. *Engineering Structures* 2010; **32**(10):3394–3403.
24. Shrestha KC, Araki Y, Nagae T, et al. Effectiveness of superelastic bars for seismic rehabilitation of clay-unit masonry walls. *Earthquake Engineering and Structural Dynamics* 2013; **42**:725–741.
25. Zhu S, Qiu CX. Incremental dynamic analysis of highway bridges with novel shape memory alloy isolators. *Advances in Structural Engineering* 2014; **17**(3):429–438.
26. Ozbulut OE, Hurlebaus S. Application of an SMA-based hybrid control device to 20-story nonlinear benchmark building. *Earthquake Engineering and Structural Dynamics* 2012; **41**(13):1831–1843.
27. Dolce M, Cardone D, Ponzo FC, Valente C. Shaking table tests on reinforced concrete frames without and with passive control systems. *Earthquake Engineering and Structural Dynamics* 2005; **34**(14):1687–1717.
28. Zhu S, Zhang Y. Seismic analysis of concentrically braced frame systems with self-centering friction damping braces. *ASCE Journal of Structural Engineering* 2008; **134**(1):121–131.
29. McCormick J, DesRoches R, Fugazza D, Auricchio F. Seismic assessment of concentrically braced frames with shape memory alloy braces. *ASCE Journal of Structural Engineering* 2007; **133**(6):862–870.
30. Motahari SA, Ghassemieh M, Abolmaali SA. Implementation of shape memory alloy dampers for passive control of structures subjected to seismic excitations. *Journal of Constructional Steel Research* 2007; **63**(12):1570–1579.
31. Yang CSW, DesRoches R, Leon RT. Design and analysis of braced frames with shape memory alloy and energy-absorbing hybrid devices. *Engineering Structures* 2010; **32**:498–507.
32. Moradi S, Alam MS, Asgarian B. Incremental dynamic analysis of steel frames equipped with NiTi shape memory alloy braces. *The Structural Design of Tall and Special Buildings* 2014; **23**(18):1406–1425.
33. Qiu CX, Zhu S. High-mode effects on seismic performance of a multi-story self-centering-braced steel frame. *Journal of Constructional Steel Research* 2016; **119**:133–143.
34. Speicher M, Hodgson DE, DesRoches R, Leon RT. Shape memory alloy compression/tension devices for seismic retrofit of buildings. *Journal of Materials Engineering and Performance* 2009; **18**:746–753.
35. Miller DJ, Fahnestock LA, Eatherton MR. Development and experimental validation of a nickel–titanium shape memory alloy self-centering buckling-restrained brace. *Engineering Structures* 2012; **40**:288–298.

DOI: 10.1002/eqe

36. Boroschek RL, Farias G, Moroni O, Sarrazin M. Effect of SMA braces in a steel frame building. *Journal of Earthquake Engineering* 2007; **11**(3):326–342.
37. Ozbulut OE, Roschke PN, Lin PY, Loh CH. GA-based optimum design of a shape memory alloy device for seismic response mitigation. *Smart Materials and Structures* 2010; **19**(6065004):.
38. Song G, Ma N, Li HN. Applications of shape memory alloys in civil structures. *Engineering Structures* 2006; **28**(9):1266–1274.
39. Ozbulut OE, Hurlebaus S, DesRoches R. Seismic response control using shape memory alloys, a review. *Journal of Intelligent Material Systems and Structures* 2011; **22**(14):1531–1549.
40. Zhu S, Zhang Y. Loading rate effect on superelastic SMA-based seismic response modification devices. *Earthquakes and Structures* 2013; **4**(6):607–627.
41. Fahnestock L, Ricles J, Sause R. Experimental evaluation of a large-scale buckling-restrained braced frame. *ASCE Journal of Structural Engineering* 2007; **133**(9):1205–1214.
42. Erochko J, Christopoulos C, Tremblay R. Design and testing of an enhanced-elongation telescoping self-centering energy-dissipative brace. *ASCE Journal of Structural Engineering* 2014; **141**(6): 04014163. doi. 10.1061/(ASCE) ST.1943-541X.0001109,04014163
43. Sommerville P, et al. (1997). Development of ground motion time histories for Phase 2 of the FEAM/SAC steel project. SAC Background Document SAC/BD-91/04, SAC Joint Venture, Sacramento, Calif.
44. Mazzoni S, Mckenna F, Scott MH, Fenves GL. OpenSees command language manual; Pacific Earthquake Engineering Research Center. 2001.
45. Erochko J, Christopoulos C, Tremblay R. Design, testing and detailed component modeling of a high-capacity self-centering energy-dissipative brace. *ASCE Journal of Structural Engineering* 2014; **141**(8): 04014193. doi. 10.1061/(ASCE)ST.1943-541X.0001166,04014193
46. "List of aftershocks of the Wenchuan earthquake exceeding M4" (in Chinese). Sichuan Quake Prevention and Disaster Reduction Information Network, by SCEA. 2008-07-18. Archived from the original on 2008-07-30. Retrieved 2008-10-25. From http://www.scdzj.gov.cn/zt/kzjzzzcc/wcdz4jml/
47. Zhang Y, Camilleri JA, Zhu S. Experimental characterization of mechanical properties of copper-based superelastic alloy at cold temperatures for the seismic protection of bridges. *Smart Materials and Structures* 2008; **17**(2025008):.

DOI: 10.1002/eqe